Geomechanics and Engineering, *Vol. 37, No. 2 (2024) 167-178*
https://doi.org/10.12989/gae.2024.37.2.167

Analytical framework for natural frequency shift of monopile-based wind turbines under two-way cyclic loads in sand

Yang Wang*[1], Mingxing Zhu[2], Guoliang Dai[3], Jiang Xu**[4] and Jinbiao Wu[5]

[1]*School of Civil and Architectural Engineering, Shandong University of Technology, Zibo, China*
[2]*School of Civil Engineering and Architecture, Jiangsu University of Science and Technology, Zhenjiang, China*
[3]*School of Civil Engineering, Southeast University, Nanjing, China*
[4]*Institute of Geotechnical Engineering, Yangzhou University, Yangzhou, China*
[5]*School of Resource and Safety Engineering, Central South University, Changsha, China*

(*Received September 12, 2023, Revised March 17, 2024, Accepted April 2, 2024*)

Abstract. The natural frequency shift under cyclic environmental loads is a key issue in the design of monopile-based offshore wind power turbines because of their dynamic sensitivity. Existing evidence reveals that the natural frequency shift of the turbine system in sand is related to the varying foundation stiffness, which is caused by soil deformation around the monopile under cyclic loads. Therefore, it is an urgent need to investigate the effect of soil deformation on the system frequency. In the present paper, three generalized geometric models that can describe soil deformation under two-way cyclic loads are proposed. On this basis, the cycling-induced changes in soil parameters around the monopile are quantified. A theoretical approach considering three-spring foundation stiffness is employed to calculate the natural frequency during cycling. Further, a parametric study is conducted to describe and evaluate the frequency shift characteristics of the system under different conditions of sand relative density, pile slenderness ratio and pile-soil relative stiffness. The results indicate that the frequency shift trends are mainly affected by the pile-soil relative stiffness. Following the relevant conclusions, a design optimization is proposed to avoid resonance of the monopile-based wind turbines during their service life.

Keywords: monopile; natural frequency; shift; soil deformation; two-way cyclic loads

1. Introduction

Global carbon neutrality is accelerating the birth of a new round of energy revolution characterized by low carbon, in which offshore wind power carries a major mission. Monopiles are one of the commonly used foundation forms of offshore wind turbines (OWTs) due to their simple installation, low cost and adaptability in most soil conditions (Barari *et al*. 2021, Zou *et al*. 2022). Monopile-based OWTs are subjected to a large number of cyclic loads, which makes them highly dynamic sensitive. Fig. 1 plots the typical forcing frequencies applied to a three-bladed OWT, including environmental excitations from wind and waves, the 1P frequency caused by rotor rotation, and the 3P frequency triggered by three blades passing (Cui and Bhattacharya 2016, DNV 2021, Niu *et al*. 2023). To avoid resonance, the natural frequency of OWTs should be kept away from these forcing frequencies. The accepted safe regions of the natural frequency could be lie in three possible intervals: 'soft-soft', 'soft-stiff' and 'stiff-stiff'. In practice, the 'soft-stiff' frequency region is generally adopted in optimization design for its satisfactory reliability and cost savings (Andersen *et al*. 2012, Gao *et al*. 2024).

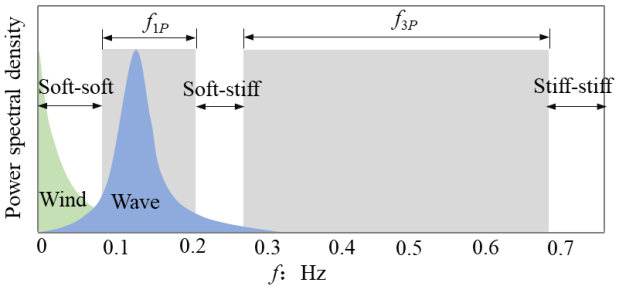

Fig. 1 Forcing frequencies plotted against power spectral density for a three-bladed OWT

Maintaining the natural frequency of whole system in the 'soft-stiff' security region during service is an essential but difficult task, as the natural frequency often varies with the long-term cyclic loads. This phenomenon has already been observed and confirmed in field and small-scale modeling experiments. Kuhn (2000) reported that the target design frequency of an OWT at the Lely wind farm was 0.4 Hz, which increased to 0.63 Hz after 6 operational years. At the Hornsea Wind Farm, it was found that the natural frequency of the OWT was reduced from 1.23 to 1.13 Hz after 3 months of operation (Lowe 2012). Nor´en-Cosgriff and Kaynia (2021) analyzed the measurement data from a wind farm in the North Sea with monopile foundations, and concluded that the long-term pile-soil interaction is an important contributor to observed changes in the the first natural frequency. Increasing or decreasing frequency are

*Corresponding author, Ph.D.
E-mail: wangyang@sdut.edu.cn
**Corresponding author, Ph.D.
E-mail: yzujxu@yzu.edu.cn

ISSN: 2005-307X (Print), 2092-6219 (Online)

strongly depended on density of sand. Small-scale model tests by Bhattacharya *et al*. (2012), Lombardi *et al*. (2013) and Lin *et al*. (2020) showed that the natural frequency of OWT in loose and medium-dense sand changed with cyclic loading, mainly due to changes in foundation stiffness as a result of gradual densification of the surrounding sandy soils. Large-scale tests carried out by Prendergast and Igoe (2022) in dense sand revealed that the monopile frequency after cycling tends to decrease due to a gradual reduction in foundation stiffness of the sandy soils with cumulative strain. Overall, the important role played by the cyclic pile-soil interaction in the variation of the natural frequency of OWTs needs to be given sufficient attention for structural health, economic and safety reasons.

To predict natural frequency with acceptable accuracy, different calculation methods considering the pile-soil interaction were proposed to estimate the natural frequency of monopile-based systems. The foundation stiffness was interpreted by several numerical models, including uncoupled stiffness (Adhikari and Bhattacharya 2011, Andersen *et al*. 2012), coupled stiffness (Arany *et al*. 2015, 2016) and p-y springs (Carswell *et al*. 2016, Gao *et al*. 2023, He *et al*. 2023). Arany *et al*. (2016) derived a closed-form solution for the natural frequency of the monopile system based on a simple cantilever beam model. Three foundation stiffness correction coefficients were introduced to realize the integrated analysis of soil-foundation-structure system. Prendergast and Gavin (2016) performed small-strain vibration tests on two monopiles and compared the frequency results with those calculated by five different foundation reaction stiffness models. Alamouti *et al*. (2017) used a Rayleigh method to derive the natural frequency of a rigid pile system and introduced an innovative procedure to account for pile flexibility. Furthermore, Yu and Amdahl (2023) present a Rayleigh-Ritz solution for evaluating natural frequencies of monopile-based OWTs by modeling soil conditions with equivalent cross coupled springs. Although there have been many studies on the frequency calculation of monopile-based OWT systems, most of them are limited to the static first-order natural frequency and fail to consider the effect of frequency shift caused by changes in the mechanical properties of the soil body.

Changes in soil mechanical properties or foundation stiffness are closely related to the soil deformation around the pile under cyclic loading. Cuéllar (2011) described in detail the process of soil deformation (densification and subsidence) around piles in saturated sandy soils by means of model tests with nearly 5 million loading cycles. Two generalized models were employed to outline the macroscopic morphology of the subsidence and densification zones. Based on the results of this research, the effect of soil deformation around piles on the foundation stiffness is further analyzed. Soil densification increases the foundation stiffness, while soil subsidence leads to a decrease in the pile embedment depth, thus weakening the stiffness of the whole system. Thus, the combined effect of subsidence and densification is integral to changes in foundation stiffness. However, there is still a gap in the study of this mechanism.

In this paper, a theoretical framework is presented for analyzing the natural frequency shift (NFS) law of monopile wind turbines under two-way cyclic loads. First, three geometric models (two originated from Cuéllar's study (2011) and one newly proposed in this paper) describing the subsidence pit and densified region are presented. Then, the changes in soil parameters due to cyclic loading are quantified based on the principle of mass conservation for subsiding and dense soils. Finally, changes in natural frequency are calculated using the method of Arany *et al*. (2016). A parametric study is conducted to investigate the effects of pile slenderness ratio, soil density and relative pile-soil stiffness on the NFS of the OWT system.

2. The establishment of theoretical framework

2.1 Description of soil deformation around piles under two-way cyclic loads

Due to the flow characteristics of sandy soils (especially the loose and medium-dense sand), the soil around the monopile is prone to continuous deformation under cyclic loads, which affects the cyclic responses of the monopile. This has been reported by many researchers (Nicolai *et al*. 2017, Abadie *et al*. 2019, Zeng *et al*. 2023) and has attracted increasing attention. Cuéllar (2011) described two idealized geometric models of soil deformation around the pile under two-way cyclic loads, whose 3-dimensional (3*D*) contours are plotted in Figs. 2(a) and 2(b), respectively. The zone enclosed by the red dashed line is the subsidence pit, which is roughly an inverted conical observed by several experimental studies (Ma *et al*. 2021, Rathod *et al*. 2021). The densified area is outlined as two geometric models, including double-cone (Fig. 2(a)) and cone frustum (Fig. 2(b)). The “real” geometry of densified area was captured by some microscopic studies through the 2*D* particle image velocimetry observations and discrete element method (DEM) simulations (Cui and Bhattacharya 2016), which provided an insight into the rationality of two models.

However, a number of experimental studies (Zorzi *et al*. 2017, Li *et al*. 2020) have shown that ratcheting convective units in the shallow soil layers around the monopile under cyclic loads occupy the densification core, while deeper densification is not significant. This conclusion supports the possibility of an alternative model, the single-cone model, as shown in Fig. 2(c). Apparently, this model is a version that removes the lower cone from the double-cone model. As far as the current study is concerned, it is not available to clarify which of the three models (i.e., the double cone, cone frustum and single cone) is more reasonable, or the target conditions for the applicability of each. Therefore, the subsequent analysis in this paper will be conducted for all models.

It should be pointed out that the above three models are geometrically symmetric along the central axis and are typically triggered by two-way cyclic loads, such as daily wind and waves in the marine environment (Rudolph *et al*. 2014). In contrast, one-way cyclic loads (e.g., extreme storms) will produce asymmetric soil deformation results

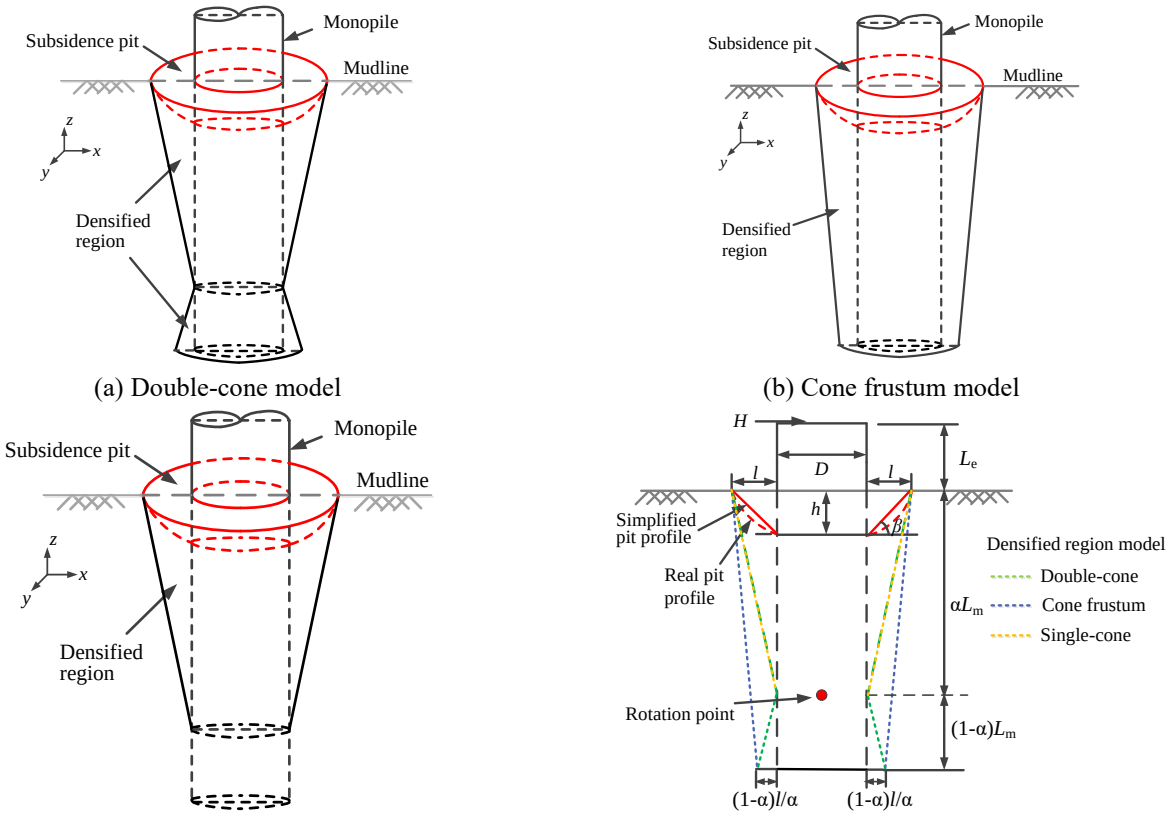

(a) Double-cone model (b) Cone frustum model

(c) Single-cone model (d) Simplified 2*D* profiles of three models

Fig. 2 Diagram of soil deformation model around monopile

(Lu and Zhang 2020). Predicting complex asymmetric soil deformation patterns under one-way cyclic loading is extremely challenging and beyond the scope of this paper.

2.2 Derivation of the relationship between the subsidence pit and densified region

For the practicality of the investigation, it is necessary to abandon rigorous modeling of soil deformation in several respects. As in a previous study (Wang *et al*. 2022), several assumptions are introduced here and simplified 2*D* profiles of the three models are integrated in Fig. 2(d), where the green, blue and orange dotted lines represent the double cone, cone frustum and single cone model, respectively.

(1) The slopes of the subsidence pits are assumed to be simple linear surfaces (Fig. 2(d)). Slope inclination β is equal to soil friction angle φ to ensure slope stability.

(2) The pile presents rigid behavior under lateral loading. The depth of the rotation point z_r is expressed as

$$z_r = \alpha L_m \tag{1}$$

where α is a coefficient depending on the pile embedded depth L_m and load eccentricity L_e, and is calculated below (Darvishi *et al*. 2017)

$$\alpha = \frac{3L_m + 4L_e}{4L_m + 6L_e} \tag{2}$$

For the double-cone and cone frustum model, if the soil subsidence length at the mudline is l, the dense width of the pile base extends laterally to $(1\text{-}\alpha)l/\alpha$ according to the principle of geometric similarity, as shown in Fig. 2(d).

(3) It is assumed that the sand densification in the area is uniform, meaning that the sand densities are the same within the densification domain.

(4) After the subsidence pit is formed, the effect of the soil above the bottom of the subsidence pit is not considered. In fact, the effect of this part of the soil on the lateral response of the pile foundation is negligible, which has been confirmed in previous scour studies (Lin and Lin 2019).

Based on the above assumptions, the following simple derivation can be carried out. In Fig. 2(d), the diameter of the top surface of the subsidence cone is $S=D+2l$ (D is the pile diameter) and the depth is $h=l\tan\varphi$. The soil subsidence volume ΔV can be calculated as the volume of the subsidence cone minus the volume of the internal pile, which is expressed as follows

$$\Delta V = l^2\pi\left(\frac{l}{3} + \frac{D}{2}\right)\tan\varphi \tag{3}$$

The volume of the densified region (V_i, i = 1, 2 and 3 refer to double-cone, cone frustum and single-cone model, respectively) can be obtained by subtracting the volume of pile and soil subsidence from the total volume wrapped by the dotted line in Fig. 2(d). The calculation results are listed as follows

$$V_1 = \pi l L_m \left(\frac{3\alpha^2 - 3\alpha + 1}{3\alpha^2} l + \frac{2\alpha^2 - 2\alpha + 1}{2\alpha} D \right) - \Delta V \quad (4)$$

$$V_2 = \pi l L_m \left(\frac{\alpha^2 - \alpha + 1}{3\alpha^2} l + \frac{1}{2\alpha} D \right) - \Delta V \quad (5)$$

$$V_3 = \pi l L_m \alpha \left(\frac{1}{3} l + \frac{1}{2} D \right) - \Delta V \quad (6)$$

Soil settlement and densification occur simultaneously, and there is a mass conservation relationship between them, with the following expression

$$\rho_0 \Delta V = V_i (\rho - \rho_0) \quad (7)$$

where ρ_0 is the initial sand density and ρ is the sand density after densification.

From Eq. (7), the densified sand density ρ can be easily obtained when the initial density ρ_0 is known.

$$\rho = \rho_0 (1 + \frac{\Delta V}{V_i}) \quad (8)$$

With the determination of sand density ρ, the relevant soil parameters are easily obtained. The sand relative density D_r can be found by using the following equation

$$D_r = \frac{(1 + e_{max})\gamma' - (G_s - 1)\gamma_w}{(e_{max} - e_{min})\gamma'} \quad (9)$$

where e_{max} and e_{min} are the maximum and minimum void ratio, respectively; G_s is the specific gravity of the soil; γ' ($=\rho g$, g is gravity) is the soil effective weight; and γ_w is the unit weight of water.

Following this, the relationship between the sand Dr and friction angle φ is clarified by Eq. (8) (Carswell *et al*. 2015).

$$D_r = 0.0014\varphi^2 - 0.0594\varphi + 0.918 \quad 0.4 \leqslant D_r \leqslant 0.8 \quad (10)$$

And the subgrade reaction coefficient n_h related to the sand friction angle or relative density is expressed as (API 2020)

$$n_h = (0.008085\varphi^{2.45} - 26.09)10^3 \quad 29^o \leq \varphi \leq 45^o \quad (11)$$

Based on the above derivation, it can be specified that that the subsidence length l is a key factor in determining the variation of soil parameters. According to previous studies (Chong and Santamarina 2016, Chong *et al*. 2019), l gradually increases with the process of loading cycles until the sand reaches the its terminal density. Hence, a dimensionless form (l/D, the ratio of subsidence length to pile diameter) is defined for the research convenience. For a pile-soil system with the initial parameters (e_{max}, e_{min}, G_s, D_r, D, L_m and L_e), the maximum value of l/D can be obtained by joining Eqs. (1)-(10) when the D_r reaches 100%. Under the premise of determining the maximum value of l/D, different values of λ can be set to express the cycle time-history process. For example, when λ = 0.25, it means that the subsidence length reaches 0.25 times of the maximum l/D. Where λ=0 represents the initial state without subsidence occurring.

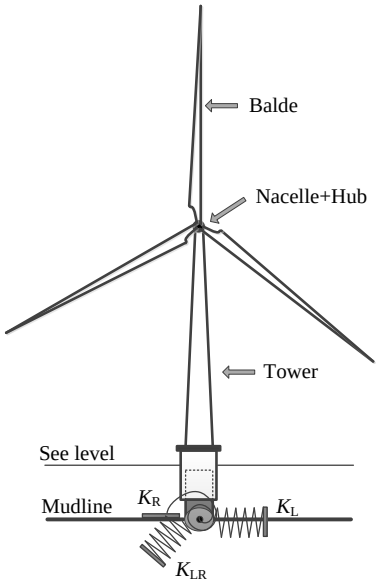

Fig. 3 Simplified OWT model with three foundation springs

2.3 A review of the analytical method for determining natural frequency

The analytical method developed by Arany *et al*. (2016) has the advantages of simplicity, parameter clarity, and comprehensive consideration of the soil-foundation-structure system, and is therefore used to calculate the system natural frequency in this paper. For the simplified OWT model in Fig. 3, the expression of the natural frequency f_0 is as follows

$$f_0 = C_L C_R C_S f_{FB} \quad (12)$$

where f_{FB} is fixed base frequency of the tower. C_L and C_R are the lateral and rotational foundation flexibility coefficients, respectively, and C_S is the substructure flexibility coefficient. Detailed explanations of f_{FB}, C_L, C_R and C_S are given in Appendix A. Among them, the correction coefficients C_L and C_R depend on foundation lateral stiffness K_L, rotational stiffness K_R and cross-coupled stiffness K_{LR}, as shown in Fig. 3. In this study, these foundation stiffnesses (K_L, K_R and K_{LR}) are calculated using the *p-y* curve method (API 2020).

The calculation process is as follows:

First, two computational models of a pure lateral load ($H\neq0$ and M=0) and overturning moment ($M\neq0$ and H=0) at the ground surface are carried out. The lateral displacement y_1 and rotation angle θ_1 of the pure H model can be expressed as a function of the flexibility coefficients

$$\begin{bmatrix} y_1 \\ \theta_1 \end{bmatrix} = \begin{bmatrix} I_L & I_{LR} \\ I_{RL} & I_R \end{bmatrix} \begin{bmatrix} H \\ 0 \end{bmatrix} \quad (13)$$

where I_L, I_{LR} and I_R are lateral, rotational and cross-coupled flexibility coefficients.

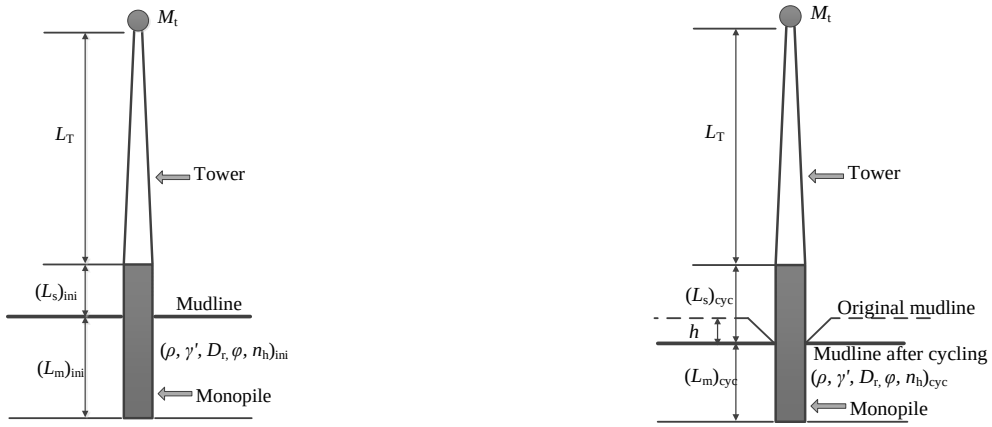

(a) Initial state (b) The state after cycling

Fig. 4 Varied parameters of the OWT system

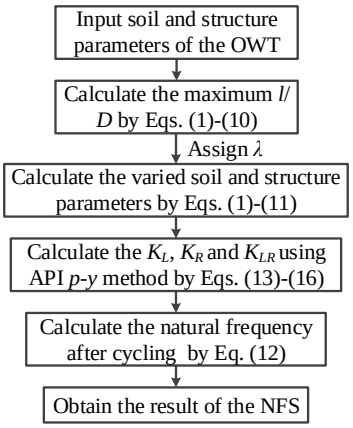

Fig. 5 Flowchart of the computing framework

Similarly, the lateral displacement y_2 and rotation angle θ_2 obtained from pure M model are expressed as

$$\begin{bmatrix} y_2 \\ \theta_2 \end{bmatrix} = \begin{bmatrix} I_L & I_{LR} \\ I_{RL} & I_R \end{bmatrix} \begin{bmatrix} 0 \\ M \end{bmatrix} \tag{14}$$

Then, from Eqs. (13) and (14), the terms of the flexibility matrix are

$$\begin{bmatrix} I_L & I_{LR} \\ I_{RL} & I_R \end{bmatrix} = \begin{bmatrix} \frac{y_1}{H} & \frac{y_2}{M} \\ \frac{\theta_1}{H} & \frac{\theta_2}{M} \end{bmatrix} \tag{15}$$

Finally, three foundation stiffnesses (K_L, K_R and K_{LR}) are obtained from the inverse relationship between the stiffness and flexibility matrix.

$$\begin{bmatrix} K_L & K_{LR} \\ K_{RL} & K_R \end{bmatrix} = \begin{bmatrix} I_L & I_{LR} \\ I_{RL} & I_R \end{bmatrix}^{-1} = \frac{1}{I_L I_R - I_{LR} I_{RL}} \begin{bmatrix} I_R & -I_{LR} \\ -I_{RL} & I_L \end{bmatrix} \tag{16}$$

2.4 Analysis procedure

Soil deformation causes the variation of the foundation stiffness, which then leads to the NFS of the OWT system. As depicted in Fig. 4, the soil parameters (ρ, γ', D_r, φ and n_h) and the structural parameters (L_m and L_s, where L_s is the distance between the mudline and the bottom of the tower) are changed after cycling due to the subsidence-densification process of the soil. For a given value of l/D or λ, the amount of change in the associated parameters can be calculated through Eqs. (1)-(11) in subsection 2.2. The natural frequency of the OWT system after cycling is determined by the method given in subsection 2.3. The complete flowchart of this computing framework is displayed in Fig. 5.

3. Verification and application of the proposed method

3.1 Validation of calculation method of natural frequency

Three OWTs are taken from different wind farm sites such as Irene Vorrink in the Netherlands, Kentish Flats in the UK and Walney 1 in the UK to evaluate the performance of the NFS computational framework for monopile-based wind turbines. These wind turbines were selected as the data, particularly the measured first natural frequency, were fully available from the relevant literatures (Arany *et al*. 2016, Amar Bouzid *et al*. 2018). The structural component parameters of the three OWT systems and the available physical properties of the soils are summarized in Table 1.

OWT structural data comes directly from the manufacturer and its accuracy can be generally guaranteed. Soil parameters are crucial for calculating the foundation stiffness. However, slight differences between some values (e.g., Poisson's ratio and shear modulus) provided by Arany *et al*. (2016) and those given in the reference (Amar Bouzid *et al*. 2018) are noticed. Also noted that there are differences in the soil density ρ provided in the literature (Arany *et al*. 2016) for the three field conditions, but the subgrade reaction coefficients are specified to be identical (n_h= 29.1 MN/m^3). According to Eqs. (10) and (11), the soil

Table 1 Physical component parameters for selecting three OWTs

Component parameters	Symbol	Unit	Irene Vorrink (Netherlands)	Kentish Flats (UK)	Walney 1 (UK)
Mass of the tower superstructure	M_t	ton	35.7	130.8	234.5
Tower mass	m_T	ton	37	108	260
Tower height	L_T	m	44.5	60.06	67.3
Tower top diameter	D_t	m	1.7	2.3	3
Tower bottom diameter	D_b	m	3.5	4.45	5
Tower density	ρ_T	kg/m^3	7850	7850	7850
Tower elastic modulus	E_T	GPa	210	210	210
Average tower wall thickness	t_T	mm	13	22	41
Distance from tower bottom to mudline	Ls	m	6	16	37.3
Monopile diameter	D	m	3.515	4.3	6
Monopile wall thickness	t_p	mm	35	45	80
Monopile embedded length	L_m	m	24.6	29.5	30
Monopile elastic modulus	E_p	GPa	210	210	210
Soil density	ρ	kg/m^2	920	920	2000
Soil poisson's ratio	v_s	-	0.5	0.4	0.4
Soil relative density	D_r	-	0.62	0.62	0.62
Soil subgrade reaction coefficients	n_h	MN/m^3	29.1	29.1	29.1
Soil shear modulus	G	MPa	55	60	70

Table 2 Flexibility parameters (I_L, I_{LR} and I_R) and corresponding stiffness parameters (K_L, K_{LR} and K_R) of three OWTs

Wind farm	I_L (m/GN)	I_R (GN^{-1})	I_{LR} (rad/(GN/m))	K_L (GN/m)	K_R (GN)	K_{LR} (GN m/rad)
Irene Vorrink	2.810	0.341	0.067	0.931	39.082	-4.741
Kentish Flats	2.057	0.214	0.036	1.274	73.033	-7.588
Walney 1	1.249	0.099	0.013	2.069	202.650	-16.033

Table 3 Comparison between the measured and calculated natural frequencies for different evaluation methods

Wind farm	Measured frequency (Hz)	Calculated frequency (Hz)			Error (%)		
		Arany *et al*. (2016)	Amar Bouzid (2018)	In this paper	Arany *et al*. (2016)	Amar Bouzid (2018)	In this paper
Irene Vorrink	0.546	0.552	0.570	0.545	+ 1.10	+ 4.39	-0.18
Kentish Flats	0.339	0.339	0.315	0.320	0	-7.08	-5.60
Walney 1	0.350	0.349	0.277	0.323	-0.40	-20.86	-7.71

relative density can be obtained (D_r = 0.62) and those soil conditions can be classified as medium-dense sand (API 2020). In the study of Amar Bouzid *et al*. (2018), the soil relative density at these three sites is 0.6, which is consistent with the mentioned results (D_r = 0.62) from the literature (Arany *et al*. 2016). In view of this, the data provided in Table 1 are considered reliable enough and are further used in the following calculations.

In accordance with subsection 2.3, the foundation flexibility coefficients (I_L, I_{LR} and I_R) and stiffness coefficients (K_L, K_{LR} and K_R) for the three field OWTs are calculated by the API *p-y* spring method (API 2020), and the results are shown in Table 2. Then using Eq. (12), the predicted natural frequencies of these systems are obtained and the results are given in Table 3. To assess the accuracy of the calculation methodology, Table 3 also lists the field measurements and the values provided by the references (Arany *et al*. 2016, Amar Bouzid *et al*. 2018). The error analysis shows that the predicted frequencies using the method of this paper are satisfactory, and slightly lower only when predicting monopiles with relatively large diameters. This may be due to the fact that the *p-y* curves used in this paper do not take into account additional soil resistance components such as skin friction, base shear and base moment (Burd *et al*. 2019, Wan *et al*. 2021).

3.2 Application of the proposed NFS framework

This part applies the proposed computational framework to the analysis of the NFS for three field cases. The analysis process employs all the soil deformation models (double-cone, cone frustum and single-cone) mentioned in subsection 2.1, which for simplicity are referred to as Model 1, Model 2 and Model 3, respectively, in the

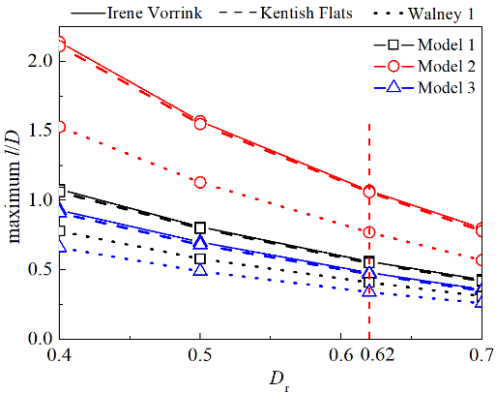

Fig. 6 Relationship between maximum *l*/D and D_r

following analysis. In addition, the analysis process requires some basic parameters of sand (including: e_{max}, e_{min}, G_s) to realize the conversion of sand D_r and ρ (see Eq. (9)). But these parameters cannot be obtained from the field data. Therefore, this study refers to the properties of a well-graded sandy soil (Fujian sand), and e_{max}, e_{min} and G_s were taken to be 0.952, 0.607 and 2.633, respectively (Ma *et al.* 2021).

Fig. 6 shows the analytical results of maximum values of *l*/*D* for three models in different D_r. The relatively dense soil (D_r>0.7) was not considered in the analysis because of its probability of dilatancy, which leads to a decrease rather than an increase in soil density (Chang and Deng 2022). It can be seen that the maximum *l*/*D* decreases as D_r increases.

This is easy to understand in that as the D_r increases, the extent of soil deformation necessarily decreases. The order of maximum *l*/*D* under the three models is Model 2, Model 1 and Model 3, which is due to the different in the volume of the dense region. An interesting phenomenon is that the curves of the two cases (Irene Vorrink and Kentish Flats) are almost identical. The reason for this may be that ratios of L_m/D is similar in both cases (L_m/D=7). While, the L_m/D of Walney is smaller (L_m/D=5) and the soil subsidence is reduced.

From Fig. 6, it can be concluded that for the three filed cases (D_r = 0.62), the maximum *l*/*D* is 0.56, 0.55 and 0.41 for Model 1, while that of Model 2 is 1.07, 1.06 and 0.77, and that of Model 3 is 0.48, 0.47 and 0.34, respectively. The products of maximum *l*/*D* and λ (= 0, 0.25 ,0.5 ,0.75 and 1) can represent the subsidence dimensions of the soil in five different stages of the cycle. The foundation stiffness (K_L, K_{LR} and K_R) for these phases can be calculated by the API *p*-*y* model. Fig. 7 shows the change ratios of the relevant parameters (K_L, K_{LR}, K_R, L_m and L_s) with respect to λ for the three filed cases. Herein the change ratios are uniformly defined as the ratio of the change value at each stage to the initial value (at λ=0). From these plots, it can be obtained that the change ratios vary approximately linearly for all parameters, with more pronounced changes in Models 1 and 2, and relatively small changes in Model 3. Among the three foundation springs, the increase in K_L is the most pronounced, followed by K_{LR} and K_R.

The natural frequency of the system increases with increasing foundation stiffness, which is referred to as the

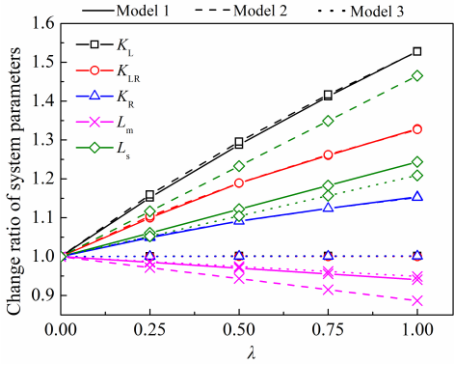

(a) Irene Vorrink

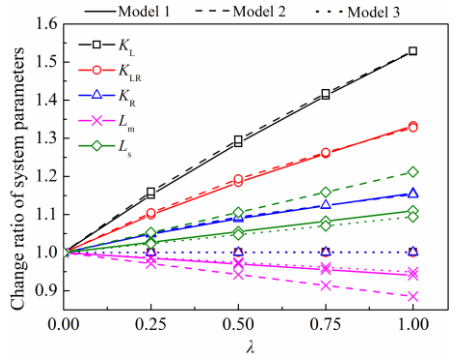

(b) Kentish Flats

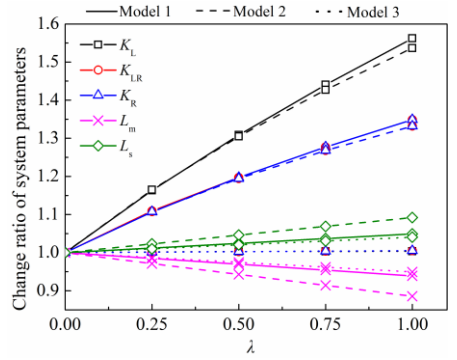

(c) Walney 1

Fig. 7 Varied K_L, K_{LR}, K_R, L_m and L_s for three filed cases

hardening effect by many researchers (Nicolai *et al.* 2017, Abadie *et al.* 2019). Comparatively, decreasing L_m and increasing L_s leads to a decrease in the system stiffness, which is considered as a softening effect. However, previous studies have often neglected this softening effect.

Fig. 8 plots the variation of the normalized natural frequency $f_\lambda/f_{\lambda=0}$ (where f_λ is the natural frequency when the subsidence reaches the stage λ and $f_{\lambda=0}$ is the initial natural frequency) with λ for three filed cases. Overall, it seems that the variation of the natural frequency in these cases is very small, less than 1.4%, which indicates that the effects of cycling-induced hardening and softening of the foundation are almost canceled out. From the comparison of the three models, Model 1 shows an increasing and then decreasing trend, while the other two models show a decreasing trend.

This indicates that the hardening effect caused by densification in Model 1 is greater than in the other two models.

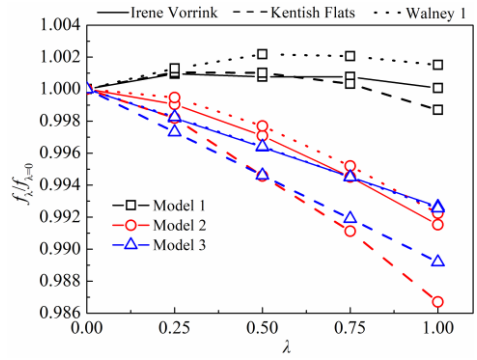

Fig. 8 The NFS for three filed cases

4. Parametric analysis and discussion

Parametric studies aim to better understand the crucial parameters of the NFS of the OWT system, so as to provide a basis for the design and optimization of structural performance. The effects of soil relative density D_r, pile slenderness ratio L_m/D and pile-soil relative stiffness on the NFS of the OWT system are investigated using the Walney 1 project as an example. Two soil relative densities were considered, loose sand (D_r=0.40) and medium dense sand (D_r=0.62). The pile slenderness ratios L_m/D are set to 3 and 5 for the rigid pile studies. Hence, there are four different working conditions corresponding to the three soil models and a total of 12 calculation scenarios.

4.1 Effect of pile slenderness ratio

Fig. 9 shows the effect of L_m/D on the NFS in loose and medium-dense sand. The different trends of the curves in both figures show the L_m/D has a significant effect on the NFS. A distinctive feature is that the natural frequency of monopiles with smaller L_m/D (=3) exhibit an increasing trend with λ. Of course, the increase is not sustainable in that the sand will eventually reach the terminal density, at which point the natural frequency also tends to stable. Comparatively, for monopiles with larger L_m/D (=5), the natural frequency mostly tends to decrease with the increment of λ.

The above phenomenon further illustrates the monopiles with smaller L_m/D tend to show hardening effect under cyclic loading, while monopiles with larger L_m/D mostly exhibits softening effect. In Fig. 9, there also exists a trend of increasing in the early stage and decreasing in the later stage, which is due to the alternation of the leading role of hardening effect and softening effect with the increase of sand density.

4.2 Effect of sand relative density

Fig. 10 reveals the effect of sand D_r on the NFS for monopiles with L_m/D =3 and L_m/D =5. It can be seen that the natural frequency of monopiles in loose sand (D_r=0.4) mostly exhibits a significant increasing trend as λ increases. This reflects the effect of progressive densification of the sand on the natural frequency of the OWT system, which is more pronounced in the loose sand than in the medium-

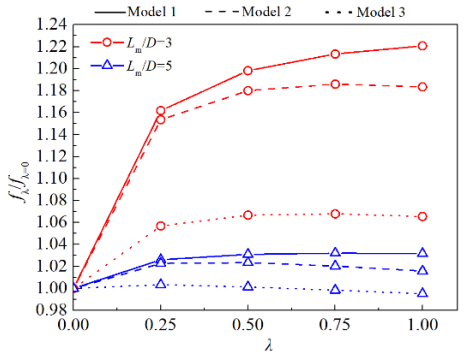

(a) Loose sand

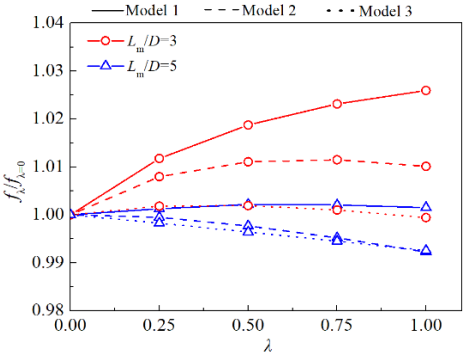

(b) Medium-dense sand

Fig. 9 Effect of L_m/D on the NFS for different sand

dense sand. Of course, there is an isolated case of L_m/D =5 monopiles in loose sand calculated by the Model 3, which first increases and then decreases to below the initial natural frequency. It is evident that the shift behavior of the OWT frequency during the cycling are very complex, reflecting the long-term competitive mechanism between the densification-induced hardening effect and the softening effect due to subsidence.

Compared to that in loose sand, it can be observed that the shift amplitude of the natural frequency in medium-dense sand (D_r=0.62) is significantly lighter, lower, with a variation of less than 1%. It can be predicted that the frequency change due to soil subsidence and densification is almost negligible when the D_r is further increased. In this case, more attention may need to be paid to the effect of dilatancy on the NFS.

4.3 Effect of pile-soil relative stiffness

The above analysis reveals that both the sand relative density and the pile slenderness ratio affect the NFS characteristics of the OWT system. In order to integrate the effects of these two parameters, the pile-soil relative stiffness coefficient T is introduced (Reese *et al*. 1974) and expressed as

$$T = \sqrt[5]{\frac{E_p I_P}{n_h}} \tag{17}$$

where E_p is the monopile elastic modulus, I_p is the inertia moment of the monopile section, and n_h is the subgrade reaction coefficient. According to Reese *et al*. (1974), the

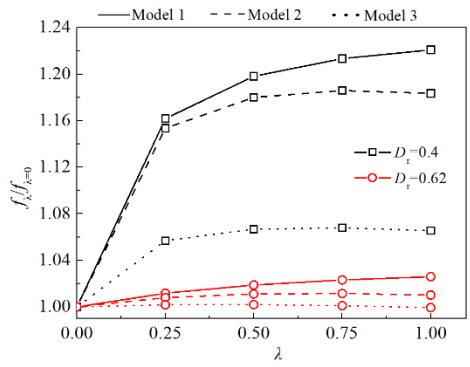

(a) L_m/D =3

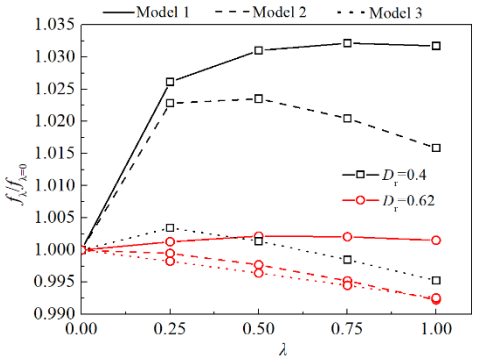

(b) L_m/D =5

Fig. 10 Effect of soil relative density D_r on the NFS for piles with different L_m/D ratios

monopile is flexible when L_m/T is greater than 5, rigid when L_m/T <2 and semi-rigid If 2<L_m/T<5.

As described above, the $f_\lambda/f_{\lambda=0}$ varies with the increment of λ. When the absolute value of $f_\lambda/f_{\lambda=0}$ reaches its maximum value (i.e., peak $f_\lambda/f_{\lambda=0}$), it can be generally regarded as the most dangerous situation. Therefore, the peak $f_\lambda/f_{\lambda=0}$ is selected as an important reference for evaluating the NFS in this study. The relationship between the peak $f_\lambda/f_{\lambda=0}$ and L_m/T for the all the above calculated cases is shown in Fig. 11. It can be seen that for L_m/T < 3, the natural frequency of the OWT system increases with cycling, and the increasing magnitude reduces with the increase of L_m/T. When L_m/T > 3, the system frequency decreases slightly, within 2%. It can also be observed that the peak $f_\lambda/f_{\lambda=0}$ computed under Model 3 are the smallest compared to Models 1 and 2, which is consistent with the findings in subsection 3.2.

From the design point of view, enough attention should be given to the rigid monopile-based OWTs due to its notable extent of NFS. In the case of a 'soft-stiff' (1*P*~3*P*) design, the design frequency should be close to the lower limit of the safety region (1*P* band) for monopiles with L_m/T <3. According to the similar principle, the design frequency of monopiles with L_m/T>3 should approach the upper limit (3*P* band).

5. Limitations of this work

This paper aims to establish a theoretical framework to evaluate the NFS of monopile-based wind turbines system

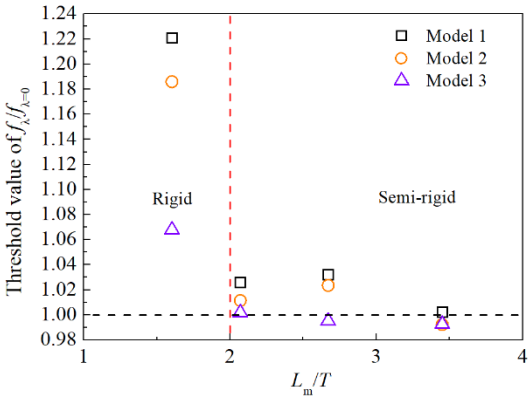

Fig. 11 Effect of pile-soil relative stiffness on the NFS

in sand under lateral cyclic loads. Given the complexity of the problem, this paper presents the following shortcomings which need to be improved in future studies.

(1) The key limitation is that only two-way cycling loads (which leads to the symmetrical sand subsidence and densification) were applied in the modeling analysis of the soil deformation around monopiles. However, one-way cycling loads occurs more frequently in marine environments and it leads to asymmetric soil deformation (Abadie *et al*. 2019, Lu and Zhang 2020). Therefore, the shift characteristics of the system frequency under one-way cycling loads leads the future direction of interest.

(2) It is widely recognized in the industry that the API *p-y* curve model is no longer suitable for calculating the lateral response of large-diameter piles. In the past few years, several multi-spring models considering additional soil resistance components such as skin friction, base shear, and base bending moment have been proposed in sandy soils (Burd *et al*. 2019, Wan *et al*. 2021). However, no agreement has been reached yet. In addition, existing *p-y* models are established based on the transverse homogeneous soil. In this study, the soil layer is anisotropic in the transverse direction due to the local densification. A new *p-y* curve considering the transverse anisotropy of soil layer should be developed in the future.

(3) Accurate field data are important for calibration and validation of the proposed NFS framework. However, real-time monitoring data for frequency change are rarely reported. Certainly, the computational results based on the proposed framework in this paper capture similar frequency trends as those reported in existing scaling tests (Lombardi *et al*. 2013, Cui and Bhattacharya 2016, Liang *et al*. 2020). Considering that the response of sand is stress-level dependent, finding a reasonable field validation remains a future effort.

6. Conclusions

In this paper, a theoretical framework is developed for evaluating the shift characteristics of natural frequencies of the monopile-based OWT system under two-way cycling loads in sand. The cause of the frequency shift is attributed to the variation of the sand around the monopile, and three

simplified geometric models are employed to describe the sand deformation, i.e., subsidence and densification. By equating the subsidence and densification soils, the relationship between the changes in soil parameters before and after cycling is quantified. The API p-y method is used to calculate the three-springs foundation stiffness, and then the system frequency is evaluated. Through case validation and multi-factor analysis, the following conclusions are drawn from this study.

- The theoretical values of system frequency calculated using the API *p-y* method fit well with the measured values of smaller-diameter monopiles in the field, and the prediction error increases as the pile diameter increases.
- Under cyclic loads, the natural frequencies of monopiles with small L_m/D (=3) usually tend to increase, showing hardening effect. The natural frequencies of larger L_m/D (=5) monopiles mostly tend to decrease and show softening effect.
- Under cyclic loads, the natural frequency of monopile in loose sand (D_r=0.4) generally shows a significant increasing trend. Compared with the loose sand, the change in natural frequency in the medium-dense sand (D_r=0.62) is significantly lighter, with a change of less than 1%.
- For $L_m/T<3$, the natural frequency of the OWT system increases with cycling, and the amplification increases as L_m/T decreases. For $L_m/T > 3$, the system frequency decreases slightly, within 2%.
- For design optimization, the design frequencies should be close to the lower limit of the safe region (1*P* band) for the OWT systems with $L_m/T<3$. The design frequencies of the OWT systems with $L_m/T>3$ should approach the upper limit (3*P* band).

Acknowledgments

The research described in this paper was financially supported by the National Natural Science Foundation of China (52078128) and Natural Science Foundation of Shandong Province (ZR2023QE172)

References

Abadie, C.N., Byrne, B.W. and Houlsby, G.T. (2019), "Rigid pile response to cyclic lateral loading: laboratory tests", *Géotechnique*, **69**(10), 1-41. https://doi.org/10.1680/jgeot.16.P.325.

Adhikari, S. and Bhattacharya, S. (2011), "Vibrations of wind-turbines considering soil-structure interaction", *Wind Struct.*, **14**(2), 85-112. https://doi.org/10.12989/was.2011.14.2.085.

API. (2020), Geotechnical and foundation design considerations, API recommended practice 2GEO, 1st edn. Washington, DC, USA: API.

Alamouti, S.D., Bahaari, M.R. and Moradi, M. (2017), "Natural frequency of offshore wind turbines on rigid and flexible monopiles in cohesionless soils with linear stiffness distribution", *Appl. Ocean Res.*, **68**, 91-102. https://doi.org/10.1016/j.apor.2017.07.009.

Amar, Bouzid, D., Bhattacharya, S. and Otsmane, L. (2018), "Assessment of natural frequency of installed offshore wind turbines using nonlinear finite element model considering soil-monopile interaction", *J. Rock Mech. Geotech. Eng.*, **10**(2), 141-154. https://doi.org/ CNKI:SUN:JRMG.0.2018-02-012.

Andersen, L.V., Vahdatirad, M.J., Sichani, M.T. and Serensen, J. (2012), "Natural frequencies of wind turbines on monopile foundations in clayey soils—a probabilistic approach". *Comput. Geotech.*, **43**(6), 1-11. https://doi.org/10.1016/j.compgeo.2012.01.010.

Arany, L., Bhattacharya, S., Macdonald, J. and Hogan, S.J. (2016), "Closed form solution of eigen frequency of monopile supported offshore wind turbines in deeper waters incorporating stiffness of substructure and SSI", *Soil Dyn. Earthq. Eng.*, **83**, 18-32. https://doi.org/10.1016 /j.soildyn.2015.12.011.

Arany, L., Bhattacharya, S., Adhikari, S., Hogan, S.J. and Macdonald, J. (2015), "An analytical model to predict the natural frequency of offshore wind turbines on three-spring flexible foundations using two different beam models". *Soil Dyn. Earthq. Eng.*, **74**, 40-45. https://doi.org/10.1016/j.soildyn.2015.03.007.

Barari, A., Zeng, X., Rezania, M. and Ibsen, L.B. (2021), "Three-dimensional modeling of monopiles in sand subjected to lateral loading under static and cyclic conditions", *Geomech. Eng.*, 26(2), 175-190. https://doi.org/10.12989/gae.2021.26.2.175.

Bhattacharya, S., Cox, J.A., Lombardi, D. and Wood, D.M. (2012), "Dynamics of offshore wind turbines supported on two foundations". *ICE- Geotech. Eng.*, **166**(2), 159-169. https://doi.org/ 10.1680/geng.11.00015.

Burd, H.J., Taborda, D.M.G. and Zdravkovic, L. (2019), "PISA design model for monopiles for offshore wind turbines: application to a marine sand", *Géotechnique*, **70**(11). https://doi.org/ 10.1680/jgeot.18.p.277.

Carswell, W., Arwade, S.R., DeGroot, D.J. and Myers, A.T. (2016), "Natural frequency degradation and permanent accumulated rotation for offshore wind turbine monopiles in clay", *Renew Energ.*, **97**(11), 319-330. https://doi.org/10.1016/j.renene.2016.05.080.

Chang, C.S. and Deng, Y. (2022), "Energy equation and stress–dilatancy relationship for sand". *Acta Geotech*., **17**, 2675-2696. https://doi.org/10.1007/s11440-021-01389-1.

Chong, S.H. and Santamarina, J.C. (2016), "Sands subjected to vertical repetitive loading under zero lateral strain: Accumulation models, terminal densities, and settlement", *Can. Geotech. J.*, **53**(12). https://doi.org/10.1139/cgj-2016-0032.

Chong, S.H., Shin, H.S. and Cho, G.C. (2019), "Numerical analysis of offshore monopile during repetitive lateral loading", *Geomech. Eng.*, **19**(1), 79-91. https://doi.org/10.12989/gae.2019.19.1.079.

Cuéllar, P. (2011), "Pile foundations for offshore wind turbines: numerical and experimental investigations on the behaviour under short-term and long-term cyclic loads", PhD thesis, Berlin, Germany.

Cui, L. and Bhattacharya, S. (2016), "Soil–monopile interactions for offshore wind turbines", *Eng. Comput. Mech.*, **169**(4), 1-12. https://doi.org/10.1680/jencm.16.00006.

DNVGL. (2021), DNVGL-ST-0126-support structures for wind turbines. Det Norske Veritas, Greater Oslo.

Gao, S.J., Feng, G.N. and Liu, F.S. (2024), "Investigation to the nonlinearity evolution of offshore wind turbines using field data: Application to a 4 MW monopile offshore wind turbine", *Appl. Ocean Res.*, **145**, 103918. https://doi.org/10.1016/j.apor.2024.103918.

Gao, Z.W., Yan, L.Y. and Whyte, S. (2023), "B-SDM: a bounding surface stiffness degradation method for modelling the long-term ratcheting response of offshore wind turbine foundations", *Comput. Geotech.*, **154**, 105157. https://doi.org/10.1016/j.compgeo.2022.105157.

He, K.P. and Ye, J.H. (2023), "Seismic dynamics of offshore wind

turbine-seabed foundation: Insights from a numerical study", *Renew Energ.*, **205**, 200-221. https://doi.org/10.1016/j.renene.2023.01.076.

Kuhn, M. (2000), "Dynamics of offshore wind energy converters on monopile foundation experience from the Lely offshore wind turbine", OWEN Workshop, CLRC Rutherford Appleton Laboratory, Swindon, UK.

Liang, R., Yuan, Y., Fu, D.F. and Liu, R. (2020), "Cyclic response of monopile-supported offshore wind turbines under wind and wave loading in sand", *Mar. Georesour. Geotech.*, **39**(10), 1230-1243. https://doi.org/ 10.1080/1064119X.2020.1821848.

Li, J., Guan, D. and Chiew, Y.M. (2020), "Temporal evolution of soil deformations around monopile foundations subjected to cyclic lateral loading", *Ocean Eng.*, **217**, 107893. https://doi.org/ 10.1016/j.oceaneng.2020.107893.

Lin, Y.J. and Lin, C. (2019), "Effects of scour-hole dimensions on lateral behavior of piles in sands", *Comput. Geotech.*, **111**, 30-41. https://doi.org/ 10.1016/j.compgeo.2019.02.028.

Lin, K., Xiao, S., Zhou, A.N. and Liu, H.J. (2020), "Experimental study on long-term performance of monopile-supported wind turbines (MWTs) in sand by using wind tunnel", *Renew Energ.*, **159**, 1199-1214. https://doi.org/ 10.1016/j.renene.2020.06.034.

Lombardi, D., Bhattacharya, S. and Wood, D.M. (2013), "Dynamic soil–structure interaction of monopile supported wind turbines in cohesive soil", *Soil Dyn. Earthq. Eng.*, **49**, 165-180. https://doi.org/10.1016/j.soildyn.2013.01.015.

Lowe, J. (2012), "Hornsea met mast-A demonstration of the 'twisted jacket' design", *Proceedings of the Global Offshore Wind Conference*, ExCel London, London, UK.

Lu, W.J. and Zhang, G. (2020), "Long-term cyclic loading tests for offshore pile foundations based on hydraulic gradient modeling". *Geotech. Test J.*, **44**(3). 686-704. https://doi.org/10.1520/GTJ20190374.

Ma, H.W., Lu, Z.Y., Li, Y.T. Chen, C. and Yang, J. (2021), "Permanent accumulated rotation of offshore wind turbine monopile due to typhoon-induced cyclic loading", *Mar. Struct.*, **80**, 103079. https://doi.org/10.1016/j.marstruc.2021.103079.

Nicolai, G., Ibsen, L.B. and White, D.J. (2017), "Quantifying the increase in lateral capacity of monopiles in sand due to cyclic loads". *Geotech. Lett.*, **7**(3). 245-252. https://doi.org/10.1680/jgele.16.00187.

Niu, X.D., Lu, G., Chen, X.G. and Wang, H.P. (2023), "A method for structural damage detection considering scour depth under the pile-soil interaction", *Mar. Struct*., **88**, 103365. https://doi.org/10.1016/j.marstruc.2022.103365.

Norén-Cosgriff, K. and Kaynia, A.M. (2021), "Estimation of natural frequencies and damping using dynamic field data from an offshore wind turbine", *Mar. Struct.*, **76**, 102915. https://doi.org/ 10.1016/j.marstruc.2020.102915.

Prendergast, L.J. and Gavin, K. (2016), "A comparison of initial stiffness formulations for small-strain soil-pile dynamic Winkler modelling". *Soil Dyn. Earthq. Eng*., **81**, 27-41. https://doi.org/10.1016/j.soildyn.2015.11.006.

Prendergast, L.J. and Igoe, D. (2022), "Examination of the reduction in natural frequency of laterally loaded piles due to strain-dependence of soil shear modulus", *Ocean. Eng*., **258**, 111614. https://doi.org/10.1016/j.oceaneng.2022.111614.

Rathod, D., Nigitha, D. and Krishnanunni, K.T. (2021), "Experimental investigation of the behavior of monopile under asymmetric two-way cyclic lateral loads", *Int. J. Geomech.*, **21**(3), 06021001. https://doi.org/10.1061/(ASCE)GM.1943-5622.0001920.

Reese, L., Cox, W.R. and Koop, F.D. (1974), "Analysis of laterally loaded piles in sand", *Proceedings of the 6th Annual Offshore Technology Conf.*, Houston. https://doi.org/ 10.4043/2080-MS.

Rudolph, C., Bienen, B. and Grabe. J. (2014), "Effect of variation of the loading direction on the displacement accumulation of large-diameter piles under cyclic lateral loading in sand", *Can. Geotech. J.*, **51**(10), 1196–1206. https://doi.org/10.1139/cgj-2013-0438

Truong, P., Lehane, B.M., Zania, V. and Klinkvort, R.T. (2019), "Empirical approach based on centrifuge testing for cyclic deformations of laterally loaded piles in sand", *Geotechnique*, **69**(2), 133-145. https://doi.org/10.1680/jgeot.17.p.203.

Wang, Y., Zhu, M.X. and Gong, W.M. (2022), "Lateral behavior of monopiles considering the effects of sand subsidence and densification under lateral cyclic loading", *Mar Georesour. Geotech.*, **40**(12), 1435-1445. https://doi.org/10.1080/1064119X.2021.2002985.

Yu, Z.L. and Amdahl, J. (2023), "A Rayleigh-Ritz solution for high order natural frequencies and eigenmodes of monopile supported offshore wind turbines considering tapered towers and soil pile interactions", *Mar. Struct.*, **92**. 103482. https://doi.org/10.1016/j.marstruc.2023.103482.

Zeng, F.H., Jiang, C. and Liu, P. (2023), "Cyclic p-y curve model of piles subjected to two-way load considering the collapse and densification of sand", *Ocean. Eng.*, **289**, 116122. https://doi.org/10.1016/j.oceaneng.2023.116122.

Zorzi, G., BaeβLer, M. and Gabrieli, F. (2017), "Influence of structural stiffness on ratcheting convection cells of granular soil under cyclic lateral loading", ES 175, 148-156.

Zou, X., Wang, Y., Zhou, M. and Zhang, X. (2022), "Simulation of monopile-wheel hybrid foundations under eccentric lateral load in sand-over-clay". *Geomech. Eng.*, **28**(6), 585-598. https://doi.org/10.12989/gae.2022.28.6.585.

GC

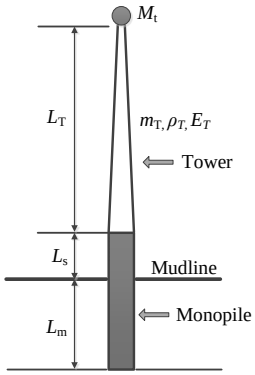

(a) Simplified elements and related structural parameters

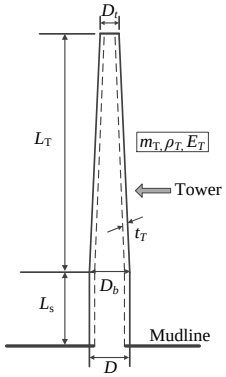

(b) Geometrical properties of the tower

Fig. A1 OWT model parameters

Appendix A

Fig. A1 plots related structural geometrical and physical parameters, and the detailed expression of relevant physical parameters in the model of Arany *et al*. (2016) is given in the following.

The natural frequency of the fixed base f_{FB} of the tower is expressed as

$$f_{FB} = \frac{1}{2\pi}\sqrt{\frac{3E_T I_T}{L^3_T(M_t + 33m_T/140)}} \tag{A.1}$$

where E_T is the elastic modulus of the tower, m_T is the mass of the tower, M_t is the total mass of the tower superstructure, L_T is the height of the tower, and I_T is the average inertia moment of the tower section, which is given by

$$I_T = \frac{1}{16}t_T\pi(D^3_b + D^3_t), \text{ in which } t_T = \frac{2m_T}{\rho_T L_T(D_b + D_t)\pi} \tag{A.2}$$

where D_t and D_b are the top and bottom diameters of the tower, respectively, and ρ_T and t_T are the density and the average wall thickness of the tower, respectively.

The correction coefficients C_L and C_R are represented by three dimensionless factors η_L, η_{LR} and η_R, as follows

$$C_L = 1 - \frac{1}{1 + 0.5(\eta_L - \frac{\eta^2_{LR}}{\eta_R})},\ C_R = 1 - \frac{1}{1 + 0.6(\eta_R - \frac{\eta^2_{LR}}{\eta_L})} \tag{A.3}$$

$$\text{in which } \eta_L = \frac{K_L L^3_T}{EI_\eta},\ \eta_{LR} = \frac{K_{LR}L^2_T}{EI_\eta},\ \eta_L = \frac{K_R L_T}{EI_\eta} \tag{A.4}$$

where K_L, K_{LR} and K_R are lateral, rotational and cross-coupling stiffness parameters, respectively. EI_η is the equivalent bending stiffness of the tower, calculated by the following equation

$$\text{in which } \eta_L = \frac{K_L L^3_T}{EI_\eta},\ \eta_{LR} = \frac{K_{LR}L^2_T}{EI_\eta},\ \eta_L = \frac{K_R L_T}{EI_\eta} \tag{A.5}$$

The correction coefficients C_S is evaluated as

$$C_S = \sqrt{\frac{1}{1 + (1+\psi)^3\chi - \chi}},\ \text{where } \chi = \frac{E_T I_t}{E_p I_P}, \psi = \frac{L_S}{L_T} \tag{A.6}$$

where L_S is the distance from the bottom of the tower to the ground surface, I_t is the inertia moment of the top section of the tower, and E_pI_p is the bending stiffness of the pile.